Supporting Information

Chromone@cucurbit[7]uril triggers the luminescence of lanthanides in water

Zhishu Zeng, Xiaodong Zhang, Guangyan Luo, Ye Meng, Lin Zhang, Weiwei Zhao, Zhu Tao and Qianjun Zhang*

Key Laboratory of Macrocyclic and Supramolecular Chemistry of Guizhou Province, Guizhou University, Guiyang 550025, China.

Email: Qianjun Zhang* - qjzhang@gzu.edu.cn.

* Corresponding author

Table of Contents

Material.....1

Apparatus.....2

Methods.....2

Host-guest interactions between CMO and Q[7].....2

L triggers the luminescence of lanthanides in water.....5

Interference and competition of metal ions.....5

Crystal structure determinations.....6

Fluorescence response of L@Eu^{3+}, L@Tb^{3+}, L@Dy^{3+} and L@Sm^{3+} to antibiotics 11

References.....12

Material

Q[7] (purity ≥97%) was prepared in the Key Laboratory of Macrocyclic and Supramolecular Chemistry of Guizhou Province, China. CMO (purity = 98%) was purchased from Shanghai Titan Technology Co., Ltd. $Eu(NO_3)_3$, $Tb(NO_3)_3$, $Dy(NO_3)_3$, $Sm(NO_3)_3$ and other reagents (purity ≥98%) were purchased from Shandong West Asia Chemical Co., Ltd. Doubly-distilled water was used throughout.

Apparatus

UV-2700 double beam UV-visible spectrophotometer; JNM-ECZ400s MHz nuclear magnetic resonance (NMR) spectrometer; Agilent 6545 Q-TOF LC/MS. VARIAN CARY ECLIPSE, Varian Cary Eclipse fluorescence spectrometer; isothermal titration calorimeter Nano ITC (TA, USA); Hamamatsu Absolute Quantum Yield Spectrometer C13534; Edinburgh FL S980; Bruker D8 VENTURE diffractometer. VERTEX70 (Bruker, Germany) Fourier infrared spectrometer.

Methods

Host-guest interactions between CMO and Q[7]

The host-guest interaction between CMO and Q[7] was investigated using UV−vis spectroscopy, ITC, MS and ^1H NMR. The interaction between Q[7] and CMO was first evaluated using UV-vis spectroscopy. The UV absorption spectrum of the interaction between CMO and Q[7] is shown in Fig. S1. CMO had strong absorption at 301 nm and the absorption intensity of CMO decreased upon increasing the concentration of Q[7]. The decrease in absorption was attributed to the host-guest interaction formed between CMO and Q[7]. In the molar ratio method, when n(Q[7])/n(CMO) approached 1.0 equivalent, the UV absorption spectrum became steady and then there was almost no significant change. In the Job's method, when n(Q[7])/[n(Q[7])+n(CMO)] = 0.5, the absorption value change reached its maximum, indicating that the ratio of CMO to Q[7]

was 1:1.

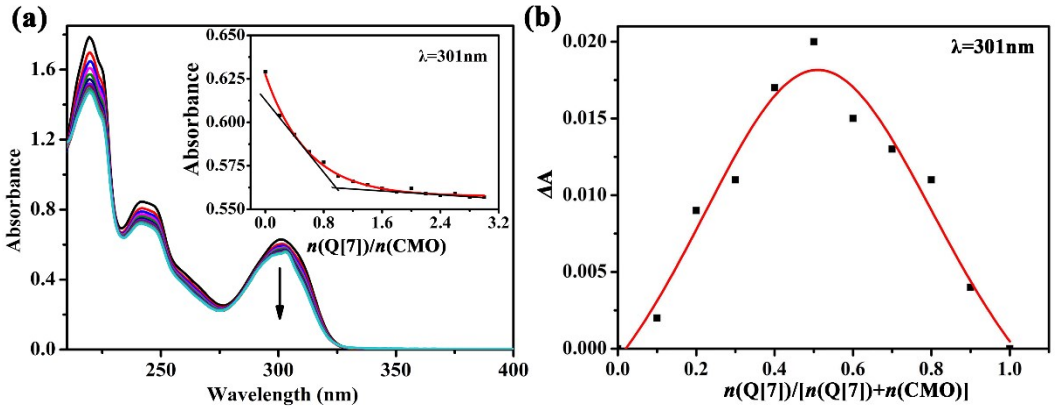

Fig. S1 UV-Vis spectra of CMO and Q[7] in an aqueous solution: (a) Molar ratio method and (b) Job's method.

Isothermal titration calorimetry (ITC) and mass spectrometry (MS) can also provide some evidence in regards to the interaction between CMO and Q[7] to support the determination of the binding constant (*K*). The ITC titration spectra and thermodynamic parameters obtained upon adding an aqueous solution of Q[7] (2.0×10^{-3} mol·L^{-1}) to an aqueous solution of CMO (1.0×10^{-4} mol·L^{-1}) at 25 °C, indicated that the inclusion process of CMO and Q[7] was mainly driven by enthalpy at a molar ratio of 1:1 and $K = 3.54 \times 10^5$ L·mol^{-1} (Fig. S2, Table S1). MS showed that the parent ion peaks of the CMO@Q[7] complex was located at *m/z* 1308.8582 $[M]^+$ (calcd.1308.3803 $[M]^+$) and 1347.5286 $[M + K]^+$ (calcd. 1347.3435 $[M + K]^+$) (Fig. S3), supporting the formation of a 1:1 inclusion complex between CMO and Q[7].

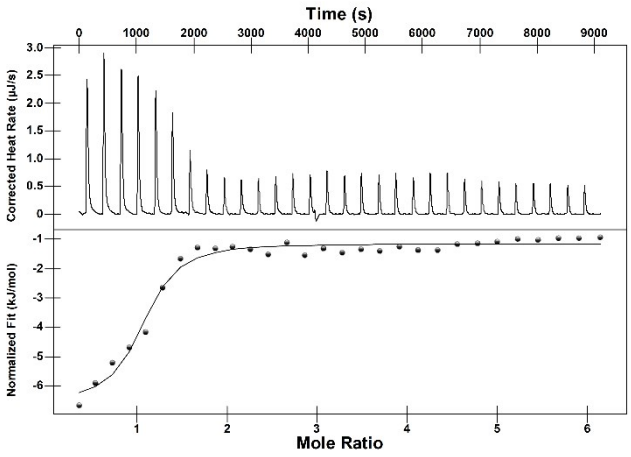

Fig. S2 ITC data obtained for the binding of Q[7] with CMO in an aqueous solution at 25 °C.

Table S1 Thermodynamic parameters related to the CMO@Q[7] system at 25 °C.

Guest-Host	*n*	*K*/(L·mol^{-1})	*ΔG*/(kJ·mol^{-1})	*ΔH*/(kJ·mol^{-1})	-*TΔS*/(kJ·mol^{-1})

CMO@Q[7]	1.01	3.54×10^5	–31.58	–6.87	–24.71

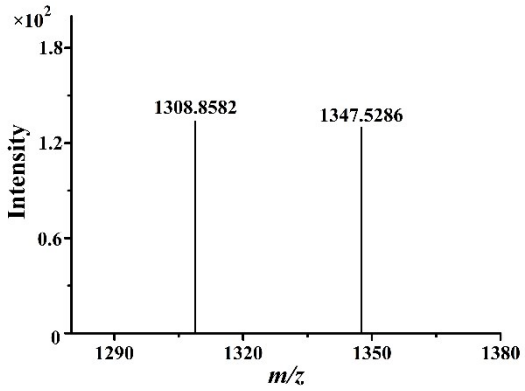

Fig. S3 ESI-TOF mass spectrometry of the CMO@Q[7] inclusion complex.

The interaction between Q[7] and CMO was further investigated using ^{1}H NMR spectroscopy. Fig. S4 and Table S2 show the changes in the ^{1}H NMR spectra of CMO, in which all the proton resonance peaks of CMO underwent an upfield shift after the addition of Q[7] in a deuterated aqueous solution. This indicated that CMO and Q[7] had a host-guest inclusion, and the whole CMO molecule entered the cavity of Q[7]. On the other hand, the addition of Q[7] caused the peaks observed for all the protons in CMO to broaden, which was due to the self-assembly and self-dissociation of the host-guest interactions occurring at the same time and the weak transition between them.

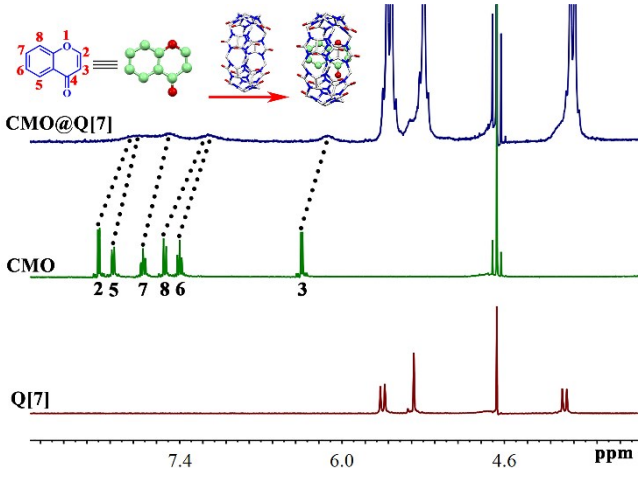

Fig. S4 ^{1}H NMR spectra (400 MHz) of CMO (5.0×10^{-4} mol·L^{-1}) in the presence and absence of Q[7] (1.0 equiv.) in D_2O.

Table S2 Changes in the ^{1}H NMR chemical shifts.

^{1}H nucleus	$\Delta\delta$/ppm
2-H	0.34
3-H	0.22
5-H	0.22
6-H	0.26
7-H	0.24

8-H	0.39

L triggers the luminescence of lanthanides in water

Fluorescence spectra were recorded on a Varian Cary Eclipse spectrophotometer. Deionized water was used as the solvent. Aqueous solutions of the L inclusion complex (3.0×10^{-5} mol·L^{-1}) and the lanthanide metal ions (La^{3+}, Pr^{3+}, Nd^{3+}, Sm^{3+}, Eu^{3+}, Gd^{3+}, Tb^{3+}, Dy^{3+}, Ho^{3+}, Er^{3+}, Tm^{3+}, Yb^{3+}, Lu^{3+}, 0.2 mol·L^{-1} stock solutions) were prepared. Known quantities of the ion solutions were added to the L inclusion complex and the fluorescence spectra were obtained by excitation at 301 nm with 10 nm emission and excitation bandwidths. Fluorescence spectra were recorded from samples in 1 cm quartz cells. Emission intensity was monitored at 300–800 nm at room temperature.

Aqueous solutions of Eu^{3+}, Tb^{3+}, Dy^{3+}, Sm^{3+} were added dropwise to aqueous L solution (3×10^{-5} mol·L^{-1}) to obtain fluorescence spectra at different ion concentrations. Absolute fluorescence quantum yields of CMO and the related complexes were measured on a Hamamatsu Absolute Quantum Yield Spectrometer C13534. The fluorescence lifetimes of L@Eu^{3+}, L@Tb^{3+}, L@Dy^{3+} and L@Sm^{3+} complexes were measured on an Edinburgh FL S980 fluorescence spectrometer. The fluorescence intensities of CMO and L were too weak to determine their lifetimes.

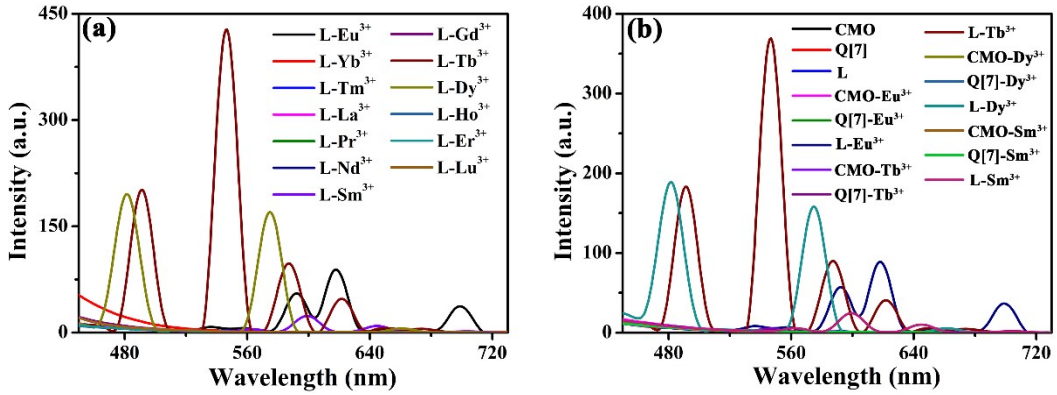

Fig. S5 (a) The effect of lanthanide series metal cations on the relative fluorescence response of L (30 μmol·L^{-1}) in water; (b) The influence of CMO, Q[7] and L on the fluorescence of four ions.

Interference and competition of metal ions

Aqueous solutions of Li^+, Na^+, K^+, Rb^+, Cs^+, Mg^{2+}, Ca^{2+}, Sr^{2+}, Ba^{2+}, Al^{3+}, Hg^{2+}, Fe^{2+}, Fe^{3+}, Cr^{3+}, Co^{2+}, Pb^{2+}, Zn^{2+}, Cd^{2+}, Ni^{2+}, Cu^{2+} and Mn^{2+} were added to the L@Eu^{3+}, L@Tb^{3+}, L@Dy^{3+} and L@Sm^{3+} systems at molar ratios of 1:1. Fluorescence measurements were recorded using an excitation wavelength of 301nm and a slit of 10:10.

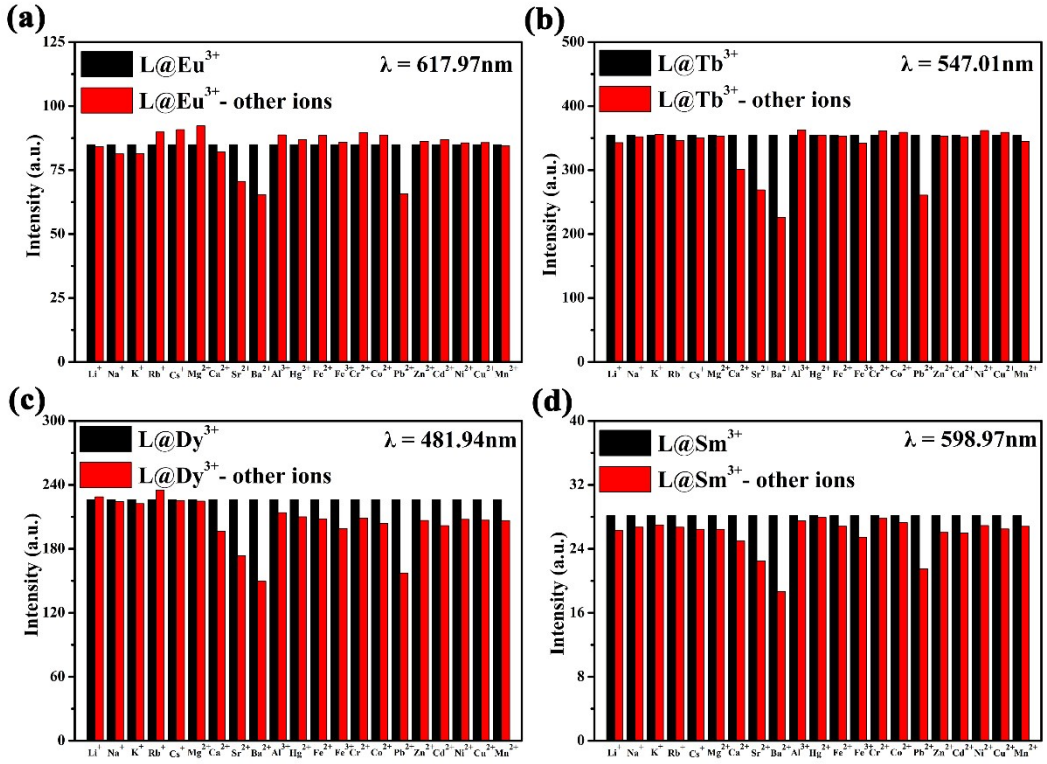

Fig. S6 The influence of other metal ions on L@Eu^{3+}, L@Tb^{3+}, L@Dy^{3+} and L@Sm^{3+} luminescence.

Crystal structure determinations

Solutions of Q[7] (0.01 g, 7.45 μmol), CMO (0.01 g, 68.43 μmol) and the lanthanide trinitrates ($Eu(NO_3)_3$, $Tb(NO_3)_3$ or $Sm(NO_3)_3$, 0.01 g, 22.42 μmol, 22.07 μmol, or 22.50 μmol, respectively) were prepared in a mixture of aqueous HCl (0.50 mL) and water (1.50 mL). Transparent crystals were obtained after standing for a period of time. The crystals were analyzed using a Bruker D8 VENTURE diffractometer.

A suitable single crystal was embedded in paraffin oil and mounted on the diffractometer, which was equipped with a graphite-monochromated Mo-Kα radiation

source (λ = 0.71055 Å) and was operated in ω-φ scan mode. Data were corrected for Lorentz and polarization effects using the SAINT program, and multi-scan absorption corrections based on equivalent reflections were also applied by using the SADABS program. The structures were elucidated through direct methods and then refined by the full-matrix least-squares method on F2 using SHELXS-97 and SHELXL-97 program packages[1,2]. All non-hydrogen atoms were refined anisotropically. Carbon-bound hydrogen atoms were introduced at calculated positions, and were treated as riding atoms with an isotropic displacement parameter equal to 1.2 times that of the parent atom. Most of the water molecules in the compounds were omitted by using the SQUEEZE option of the PLATON program. Analytical expressions for neutral-atom scattering factors were employed and anomalous dispersion corrections were incorporated. Details of the crystal parameters, data collection conditions and refinement parameters for the compounds are summarized in Table S3. In addition, the crystallographic data for the reported structures have been deposited at the Cambridge Crystallographic Data Centre as supplementary publication nos. CCDC-2051201, CCDC-2045323 and CCDC-2045329. These data can be obtained free of charge from the Cambridge Crystallographic Data Centre via www.ccdc.cam.ac.uk/data_request/cif.

Table S3 X-ray crystal data obtained for the L@Eu^{3+}, L@Tb^{3+} and L@Sm^{3+}

Complex	L@Eu^{3+}	L@Tb^{3+}	L@Sm^{3+}
Empirical formula	$\{Eu_2(H_2O)_8L_2\}$ $\{8Cl^-\}$	$\{Tb_2(H_2O)_8L_2\}$ $\{6Cl^-\}$	$\{Sm_2(H_2O)_8L_2\}$ $\{6Cl^-\}$
Formula weight	3349.99	3290.99	3275.87
Crystal system	triclinic	tetragonal	tetragonal
Space group	P -1	I 41/a	I 41/a
a[Å]	18.489(6)	44.084(7)	44.190(10)
b[Å]	18.911(6)	44.084(7)	44.190(10)
c[Å]	19.397(6)	19.521(4)	19.759(5)
α[°]	65.126(8)	90.00	90.00
β[°]	65.814(9)	90.00	90.00
γ[°]	79.368(10)	90.00	90.00
V[$Å^3$]	5612(3)	37936(15)	38585(19)
Z	1	8	8
$D_{calcd.}$[$g \cdot cm^{-3}$]	0.991	1.152	1.128
T[K]	273.15	273.15	296.0
μ[mm^{-1}]	0.710	0.896	0.757

Parameters	939	936	936
R_{int}	0.2530	0.1935	0.1407
R[I > 2σ(I)][a]	0.2342	0.0503	0.0513
wR[I > 2σ(I)][b]	0.5510	0.1321	0.1415
R(all data)	0.3307	0.0839	0.0856
wR(all data)	0.5832	0.1653	0.1802
GOF on F^2	1.539	1.093	1.184

[a] Conventional *R* on F*hkl*: $\sum||F_0| - |F_c||/\sum|F_o|$; [b] Weighted R on |F*hkl*|^2: $\sum[w(F_o^2-F_c^2)^2]/\sum[w(F_o^2)^2]^{1/2}$.

ESI-TOF mass spectrometry of the L@Eu^{3+}, L@Tb^{3+}, L@Dy^{3+} and L@Sm^{3+} systems were recorded on an Agilent 6545 Q-TOF at room temperature. Aqueous solutions of L@Eu^{3+}, L@Tb^{3+}, L@Dy^{3+}, and L@Sm^{3+} were prepared at a concentration of 1.00×10^{-4} mol·L^{-1}, the solution then filtered and then subjected to MS.

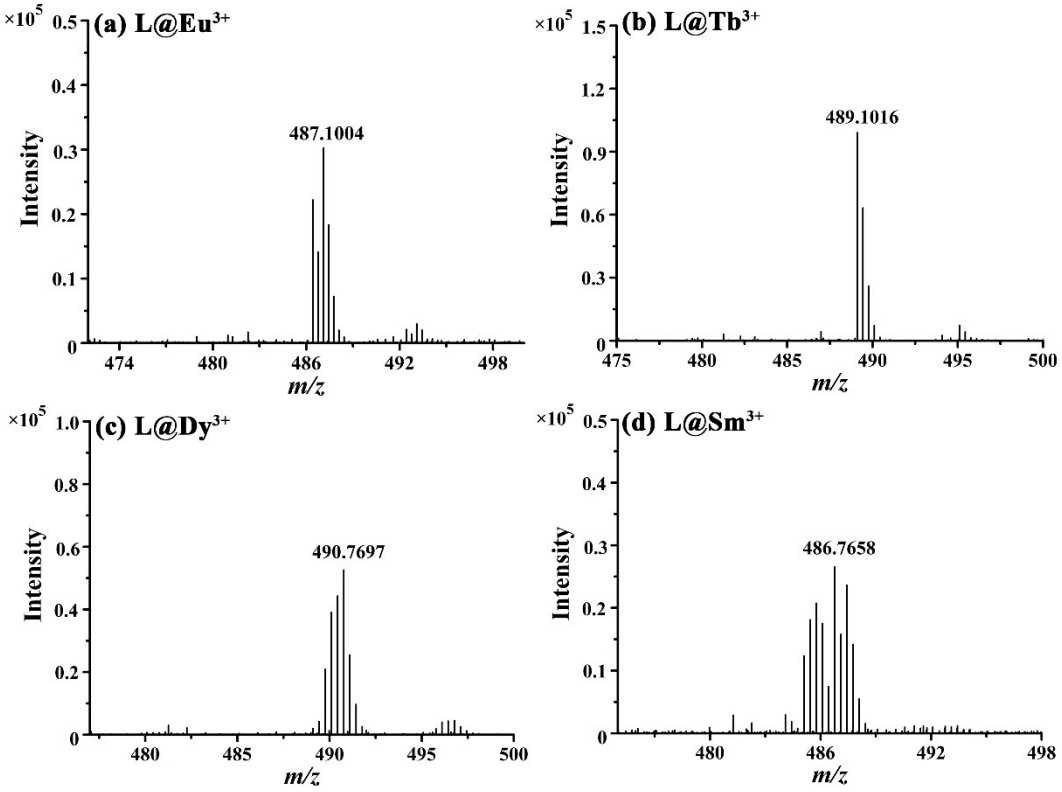

Fig. S7 ESI-TOF mass spectrometry of the L@Eu^{3+}, L@Tb^{3+}, L@Dy^{3+} and L@Sm^{3+} systems.

Infrared spectra of samples in KBr were recorded using a scanning range of 4000–500 cm^{-1}.The inclusion complexes were prepared by the method of reference.[3] The requisite amounts of CMO, Q[7], Eu^{3+}, Tb^{3+}, Dy^{3+}, Sm^{3+} were weighed according to the following ratios: *n*(CMO):*n*(Q[7]) = 1:1; *n*(CMO):*n*(Q[7]):*n*(Eu^{3+}) = 1:1:1; *n*(CMO):*n*(Q[7]):*n*(Tb^{3+}) = 1:1:1; *n*(CMO):*n*(Q[7]):*n*(Dy^{3+}) = 1:1:1; *n*(CMO):*n*(Q[7]):*n*(Sm^{3+}) = 1:1:1. The mixtures were dissolved in deionized water and

stirred for 1 h. The solvent was then evaporated to leave the L, L@Eu^{3+}, L@Tb^{3+}, L@Dy^{3+} and L@Sm^{3+} inclusion complexes.

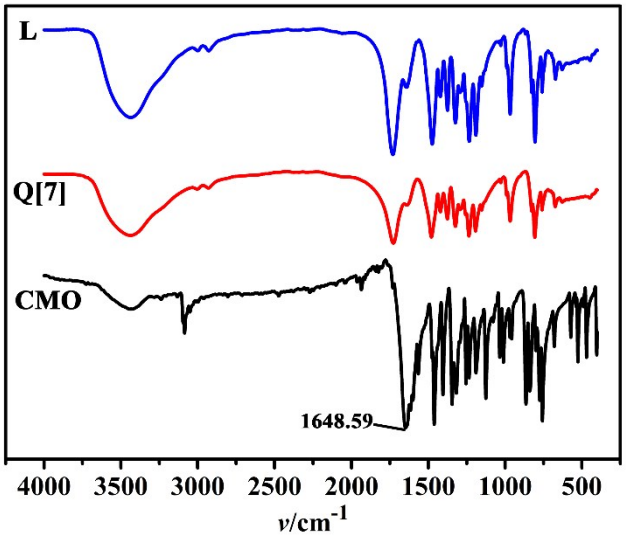

Fig. S8 IR spectra of CMO, Q[7] and L.

Thermodynamic parameters and binding constants (*K*) were determined by isothermal titration calorimetry (ITC) using a Nano ITC calorimeter (TA Instruments, New Castle, DE, USA). Solutions of Eu^{3+}, Tb^{3+}, Dy^{3+} and Sm^{3+} (1.0×10^{-3} mol·L^{-1}) and L (1.0×10^{-4} mol·L^{-1}) were prepared in deionized water. L was titrated with Eu^{3+}, Tb^{3+}, Dy^{3+}, Sm^{3+} solutions during 300 s using 30 aliquots (8 μL) at 25 °C and a stirring speed of 250 r·min^{-1} to determine the thermodynamic parameters.

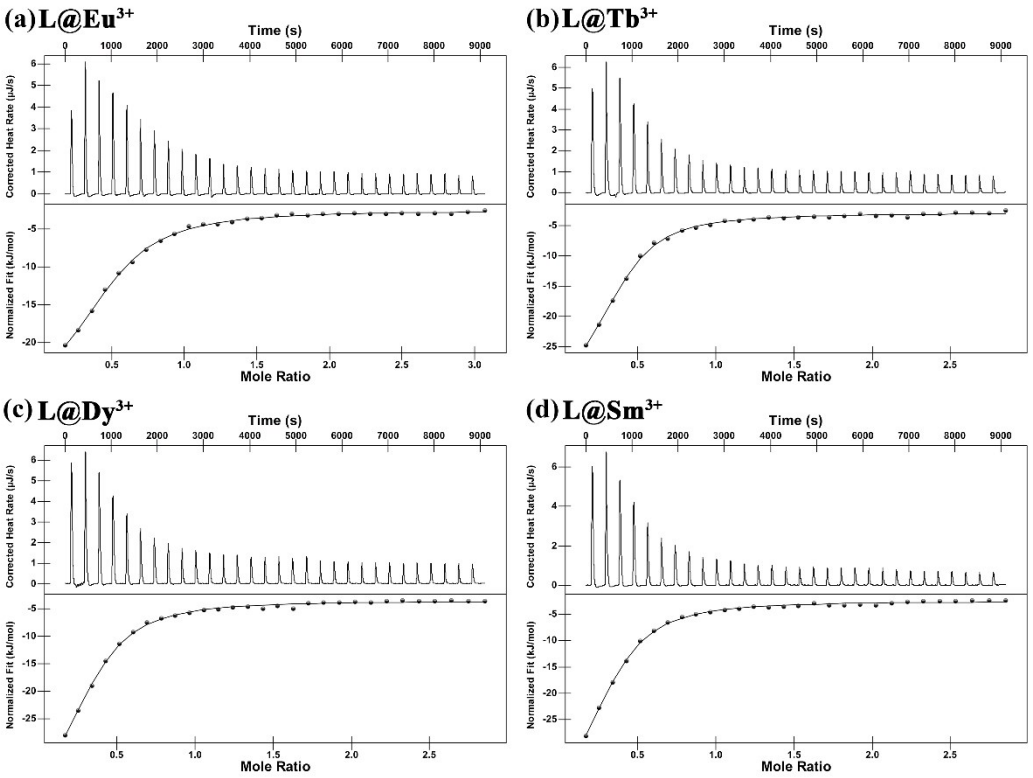

Fig. S9 ITC data obtained for the binding of Eu^{3+}, Tb^{3+}, Dy^{3+} and Sm^{3+} with L in an aqueous solution at 25 °C.

Table S4 Thermodynamic parameters of the L@Eu^{3+}, L@Tb^{3+}, L@Dy^{3+} and L@Sm^{3+} systems at 25 °C.

Complex	K/(L·mol^{-1})	ΔG/(kJ·mol^{-1})	ΔH/(kJ·mol^{-1})	$-T\Delta S$/(kJ·mol^{-1})
L@Eu^{3+}	8.34×10^4	–28.09	–25.69	–2.40
L@Tb^{3+}	1.30×10^5	–29.19	–31.19	2.00
L@Dy^{3+}	1.06×10^5	–28.69	–39.12	10.43
L@Sm^{3+}	1.08×10^5	–28.74	–41.26	12.52

The L@ Ln^{3+} complexes of L with Eu^{3+}, Tb^{3+}, Dy^{3+} and Sm^{3+} were prepared using n(L):n(Ln^{3+}) = 1:1, respectively. The SEM images were obtained on a scanning electron microscope and the elemental composition of the samples was determined using energy dispersive spectroscopy (EDS). Au Pd should be added to increase their electrical conductivity in EDS, so the *Wt*% and *At*% values are the contents obtained after the deduction of Au Pd.

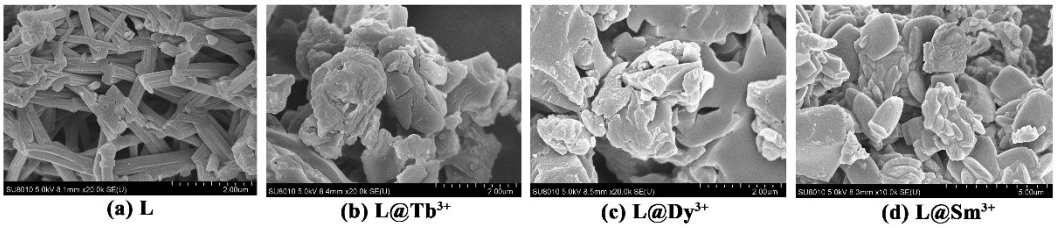

(a) L (b) L@Tb^{3+} (c) L@Dy^{3+} (d) L@Sm^{3+}

Fig. S10 The SEM image of L and the L@Eu^{3+}, L@Tb^{3+}, L@Dy^{3+} and L@Sm^{3+} complexes.

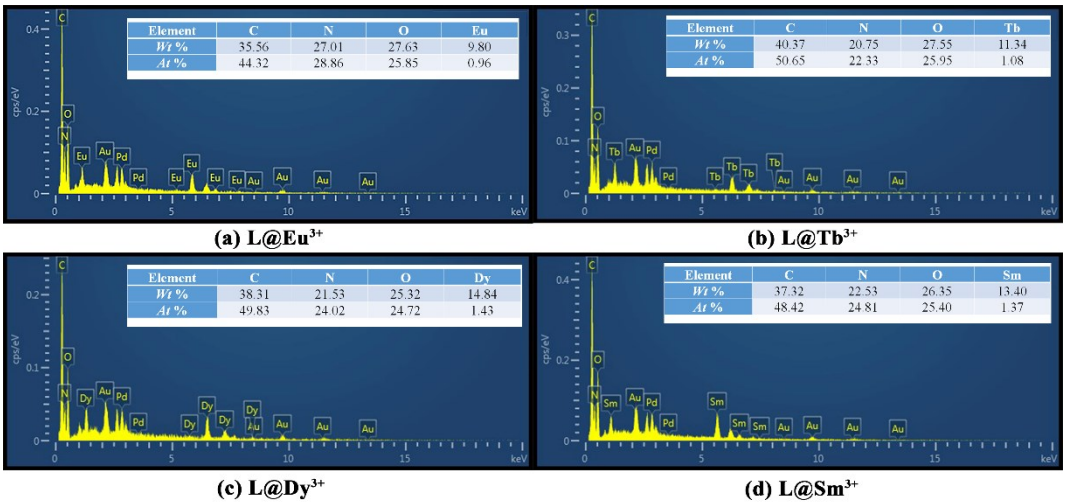

Fig. S11 The EDS element analysis of L and the L@Eu^{3+}, L@Tb^{3+}, L@Dy^{3+} and L@Sm^{3+} complexes.

Fluorescence response of L@Eu^{3+}, L@Tb^{3+}, L@Dy^{3+} and L@Sm^{3+} to antibiotics

Using a molar ratio of n(An)/n(L) = 5, different antibiotics were added to the L@Eu^{3+}, L@Tb^{3+}, L@Dy^{3+} and L@Sm^{3+} systems in aqueous solution. Fluorescence measurements were recorded using an excitation wavelength of 301nm with a slit of 10:10. The antibiotics tested included chloramphenicol (CPE), nitrofurazone (NZO), sulfadiazine (SAZ), sulfamethazine (STA), sulfamethoxazole (SMA), amoxicillin trihydrate (ARA), metronidazole (MAZ), cephalexin (CRA), trimethoprim (TOP), roxithromycin (RMY) and lincomycin hydrochloride (LOR).

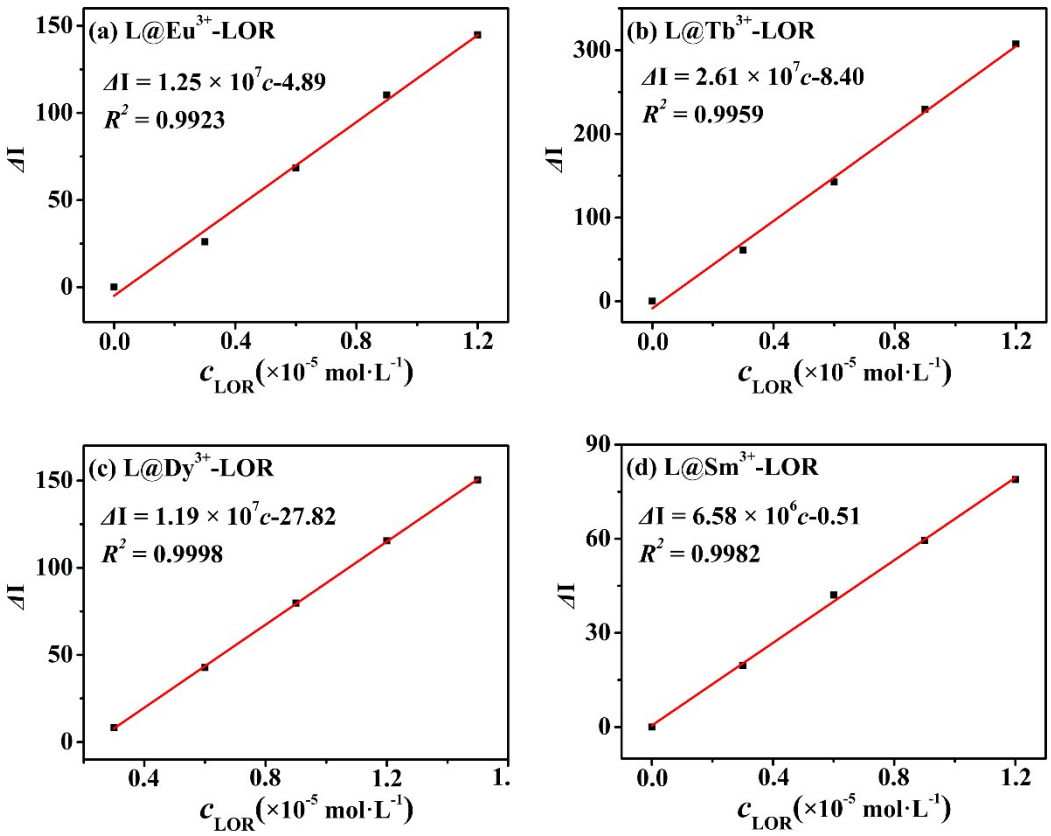

Fig. S12 The linear relationship between the fluorescence intensities of L@Eu^{3+}, L@Tb^{3+}, L@Dy^{3+} and L@Sm^{3+} and the LOR concentration.

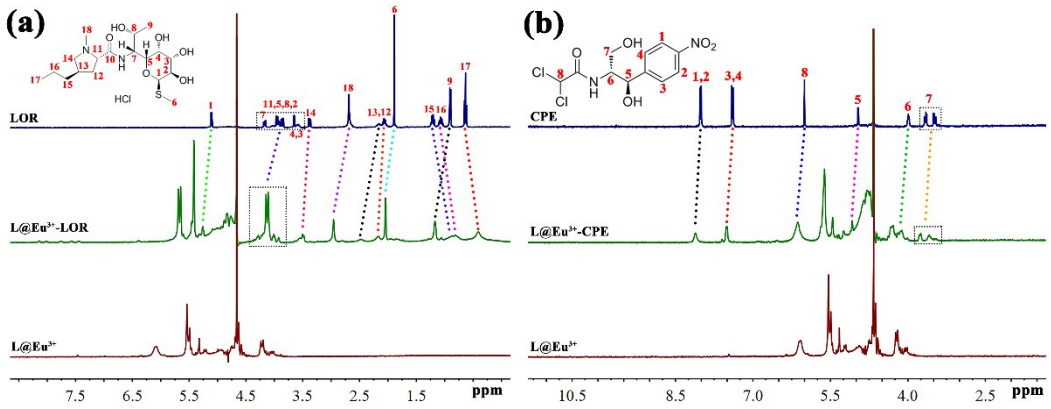

Fig. S13 The changes in the ^1H NMR spectra of L@Eu^{3+} after the addition of LOR or CPE.

References

1 G. M. Sheldrick, *Acta. Crystallogr. A.*, 2008, **64**, 112–122.

2 G. M. Sheldrick, *University of Goettingen Germany*, 1997.

3 X. D. Zhang, J. Xie, Z. L. Xu, Z. Tao, Q. J. Zhang, *Beilstein J. Org. Chem.*, 2020,

16, 71–77.